Available online at www.sciencedirect.com
SCIENCE DIRECT®
Journal of Power Sources 146 (2005) 323–326
JOURNAL OF POWER SOURCES
www.elsevier.com/locate/jpowsour

Nano-sized γ-Fe_2O_3 as lithium battery cathode

Sho Kanzaki [a], Taro Inada [a], Tadaaki Matsumura [b], Noriyuki Sonoyama [a], Atsuo Yamada [a], Mikio Takano [c], Ryoji Kanno [a,*]

[a] *Department of Electronic Chemistry, Interdisciplinary Graduate School of Science and Engineering, Tokyo Institute of Technology, 4259 Nagatsuta, Midori, Yokohama 226-8502, Japan*
[b] *Department of Chemistry for Materials, Factory of Engineering, Mie University, 1515 Kamihama-cho, Tsu 514-8507, Japan*
[c] *Institute for Chemical Research, Kyoto University, Gokasho, Uji 611-0011, Japan*

Available online 27 April 2005

Abstract

Nano-sized crystalline γ-Fe_2O_3 (particle size ca. 7 nm) was synthesized by mild oxidation of iron micelle obtained from $Fe(CO)_5$. Heat treatment at 400 °C in vacuum was effective to remove a large amount of organic impurities, the weight of which was over 40 wt.% in the as-prepared solid phase. Significant suppression of the spinel-rocksalt transformation was confirmed as the major nano-sized effect and led to the reversible topochemical lithium interaction with the corresponding lattice volume expansion.

Keywords: Heat treatment; Lithium; Spinel-rocksalt transformation

1. Introduction

Various kinds of alternative materials for lithium battery cathode have been extensively explored, mainly due to the toxicity and high cost of the present $LiCoO_2$. Abundant binary iron oxides are one of the most ideal materials in terms of its low cost and low environmental impact, and thus have been a continuous research subject since Thackeray et al. [1] have reported the chemical and electrochemical reactivity of α-Fe_2O_3 and Fe_3O_4 with lithium. However, conventional large particles of α-Fe_2O_3, Fe_3O_4 and γ-Fe_2O_3, have been considered to be difficult to serve as a cathode material for lithium secondary battery due to their irreversible transformation from columdum/spinel phase to disordered rock-salt phase [1–3].

Recently, some iron oxides with nano-sized particle have been reported to react with lithium in a reversible manner [4–9]. For example, Larcher et al. [4,5] reported drastic effect on the reactivity led by the reduced particle size, and nanometric α-Fe_2O_3 (ca. 20 nm) indicated reversibly and topotactically react with up to one Li per formula unit. Matsumura et al. [6] synthesized nano-sized α-Fe_2O_3/SnO_2 binary system (ca. 7 nm) with the SO_4^{2-} additive, and described the compound with α-Fe_2O_3: SnO_2 is 7: 3 shows a reversible capacity of 300 mAh g^{-1} based on the lithium intercalation and the surface reaction on the particle.

The structure of γ-Fe_2O_3 can be categorized into the defect spinel, in which a part of the octahedral sites in Fe_3O_4 is vacant, and may provide effective interstitial path for lithium movement. With respect to this advantageous inherent crystallographic aspect, we have decided to explore the potential performance of nano-sized γ-Fe_2O_3 as a lithium battery cathode. Of particular technical interests are (i) suppression of spinel-rocksalt transformation which have hindered the reversible redox reaction, (ii) maximizing the lithium reactivity by huge surface area, and (iii) kinetic improvement by the minimum distance for lithium to pass across the particle.

In this paper, we report the synthesis of nano-sized crystalline γ-Fe_2O_3 without impurity phase and its electrochemical activity as a lithium battery cathode. Reversible lithium intercalation without spinel-rocksalt phase transformation was confirmed.

* Corresponding author. Tel.: +81 459245401; fax: +81 459245401.
E-mail address: kanno@echem.titech.ac.jp (R. Kanno).

0378-7753/$ – see front matter © 2005 Elsevier B.V. All rights reserved.
doi:10.1016/j.jpowsour.2005.03.025

2. Experimental

Nano-sized γ-Fe_2O_3 was synthesized by mild oxidation of $Fe(CO)_5$ using the method reported by Hyeon et al. [10]. $Fe(CO)_5$ (0.5 ml) was added to a mixture of 25 ml of octylether and 1.8 ml of oleic acid, used as surfactant, at 100 °C. The solution was refluxed at 287 °C for 1 h. After cooling to room temperature, 0.85 g of dehydrated trimethylamin *N*-oxide as oxidant was added. The solution was heated again to 130 °C and the temperature was kept for 2 h. Then, the reaction temperature was slowly increased up to the reflux point, and was kept for 1 h. All the processes were performed in Ar atmosphere. After cooling to room temperature, excess ethanol was added. The black precipitate was centrifuged for isolation, and washed with ethanol. The products were characterized by transmission electron microscopy (Hitachi Co., H-9000), X-ray diffraction (Rigaku, RU-200B) and TG–DTA measurement (SII, TG/DTA6300, EXSTAR6000).

All electrochemical tests were performed at 25 °C with a stainless steel cell (HS test cell, Hosen Co.) with lithium metal as anode. The electrolyte was 1 M $LiPF_6$/ethylene carbonate:diethyl carbonate = 3:7. The cathode was a mixture of γ-Fe_2O_3:acetylene black:poly(vinilidene fluoride) (PVdF), with the weight ratio of 4:2:1. The mixture was dispersed into the *N*-methyl-2-pyrrolidinone (NMP), and the slurry was cast on Al plate to form an electrode, which was dried at 80 °C in vacuum before electrochemical tests.

3. Results and discussions

Fig. 1a shows the XRD pattern of as-prepared product. Well-defined X-ray reflections for γ-Fe_2O_3 (JCPDS number 251402) were obtained together with strong impurity peaks at low angle. This impurity phase was considered to be high molecule organic compound, such as dimer of oleic acid or oleic amide, and was hard to removed due to the lack of suitable filtering solvent. Then, we tried to isolate γ-Fe_2O_3 phase by heat treatment. The TG–DTA data shows ca. 40% of weight loss from 300 °C to 400 °C and the corresponding endothermic DTA peak around 400 °C was observed (Fig. 2). This suggests the heat treatment should be performed at $T \geqq 400$ °C. However, it is known that γ-Fe_2O_3 is transformed to α-Fe_2O_3 over 400 °C in air, so heat-treatment was performed in vacuum to prevent this transformation. Fig. 1b and c shows the XRD patterns measured for products after heat-treatment in vacuum at 400 °C and 500 °C, respectively. The γ-Fe_2O_3 phase with no impurity phase in XRD pattern was obtained after heat-treated at 400 °C, however, α-Fe metal was the main phase after heat-treatment at 500 °C. TEM images measured before/after heat-treated at 400 °C are shown Fig. 3. Very small particle size of ca. 7 nm as well as clear lattice images was observed in both pictures. These observation means that highly crystallized γ-Fe_2O_3 nanoparticles were already in the precipitates and their original characteristic were preserved after the heat treatment. To this end, the following electrochemical measurements were performed using nano-sized γ-Fe_2O_3 heat-treated at 400 °C for 6 h in vacuum.

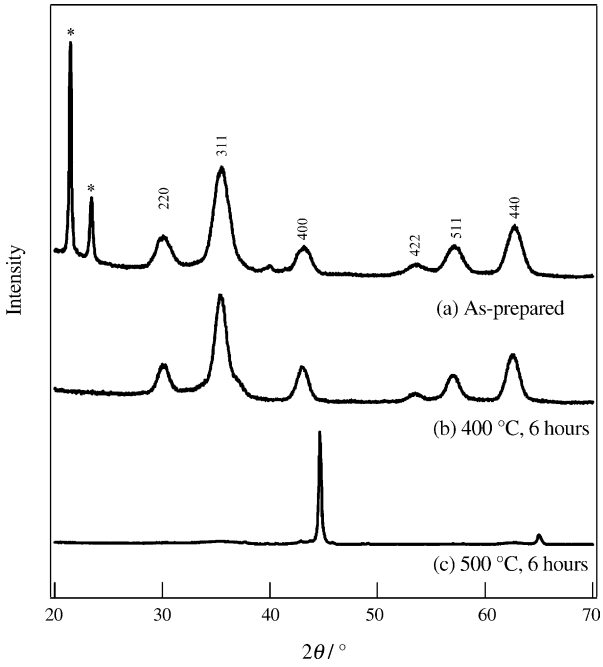

Fig. 1. X-ray powder diffraction patterns of (a) as-prepared product, (b) product after heat-treated at 400 °C in vacuum, and (c) product after heat-treated at 500 °C in vacuum. The peaks indicated by the asterisks are characteristic for the impurity phase.

Fig. 4 shows the first discharge curve for the nano-sized γ-Fe_2O_3 in comparison with one of the commercially available γ-Fe_2O_3 sample (high purity chemicals, particle size is ca. 1 μm). A large capacity can be delivered from nano-sized γ-Fe_2O_3 (230 mAh g^{-1}, ca. 1.37 mol of lithium per iron oxide) and is four times larger than the one delivered from conventional γ-Fe_2O_3 particle (55 mAh g^{-1}, ca. 0.33 mol of lithium per iron oxide). Fig. 5 shows ex situ XRD measurements for nano-sized γ-Fe_2O_3 during the first discharge process at a current density of 56.5 μA cm^{-2}. The overall shift

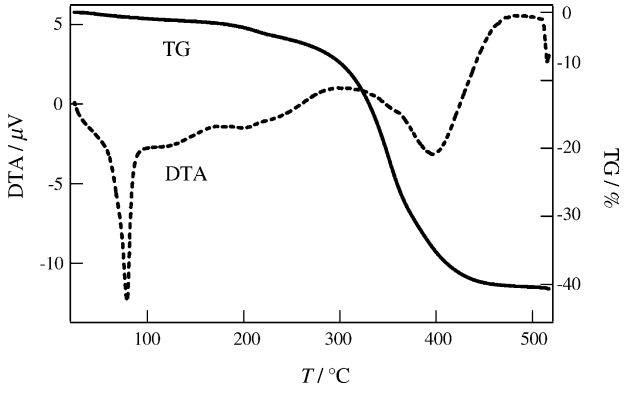

Fig. 2. TG–DTA curves of as-prepared γ-Fe_2O_3 at a heating rate of 5 °C min^{-1}.

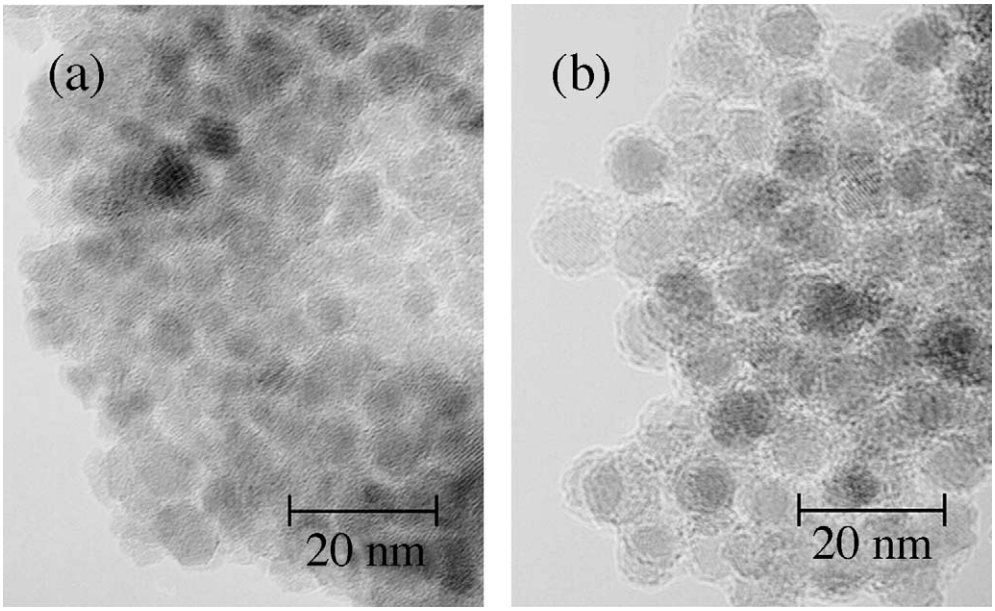

Fig. 3. TEM images of (a) as-prepared products and (b) product after heat-treated at 400 °C in vacuum.

of reflections toward low angles and the relative increase of (0 0 4) reflection intensity was observed at 1.0 V. All the XRD patterns were analyzed with a space group $P4_332$ maintaining the original framework of γ-Fe_2O_3 without nucleation or growth of another phase. The monotonic increase of the cubic lattice parameters as a function of the depth of discharge is summarized in Fig. 6, where approximately 0.25% expansion of lattice parameter (0.75% as a volume) was confirmed with an estimated ratio of $Li/Fe_2O_3 = 1.37$. Although a slight phase transformation seems to occur at the end of discharge as indicated by relative increase of (0 0 4) peak intensity in Fig. 5, the discharge process is essentially based on the topochemical reaction. The efficient downsizing of the γ-Fe_2O_3 particle leads to significant suppression of the well-known irreversible spinel-rocksalt transition reported by Pernet and Bonnet [3].

Mössbauer spectroscopy revealed that the valence state of Fe was Fe(III)/Fe(II) = 45/55 after discharge process (Fig. 7b). This value corresponding to 193 mAh g^{-1} as a capacity, which is lower than the measured capacity of 230 mAh g^{-1}. This result indicates that some residual current is consumed to cause parasite reaction other than the lithium intercalation. The small bump around 1.5 V observed in the discharge curves in Fig. 3 may correspond to the decomposition of electrolyte to form solid electrolyte interface (SEI) at

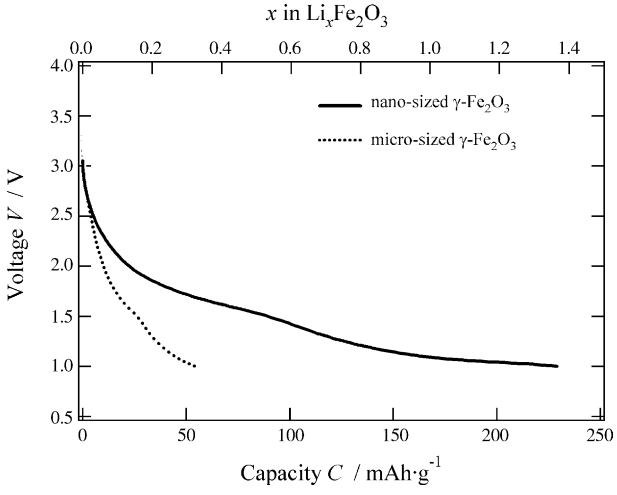

Fig. 4. First discharge curves for nano-sized γ-Fe_2O_3 (particle size: 7 nm) and commercial γ-Fe_2O_3 (particle size: 1 μm). Conditions: cut-off voltage, 1.0 V; current density, 0.1 mA cm^{-2}.

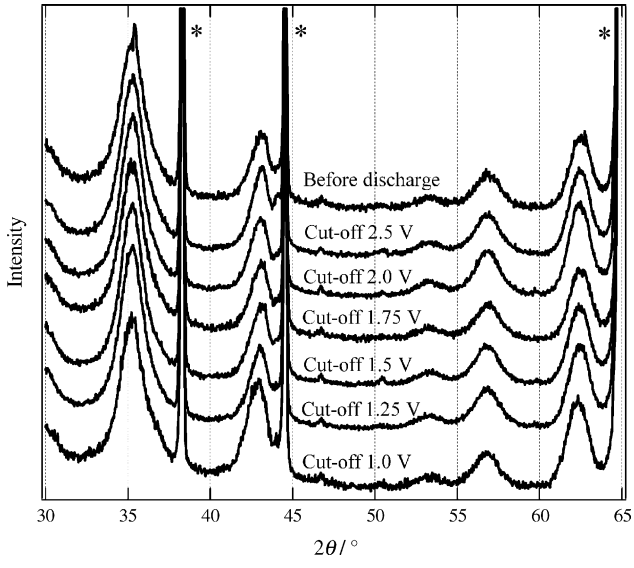

Fig. 5. Ex situ X-ray diffraction patterns of nano-sized γ-Fe_2O_3 measured during the first discharge process. The discharge current density was 56.5 μA cm^{-2}. The peaks with asterisk label are diffractions from the Al current collector.

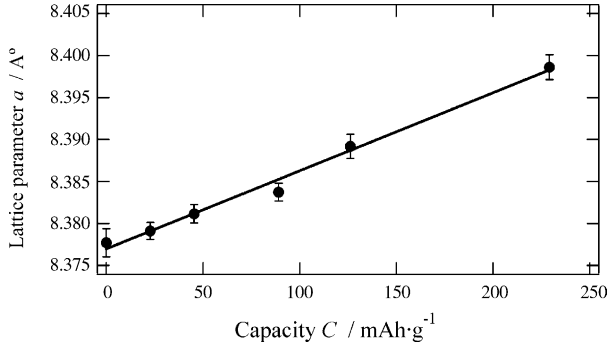

Fig. 6. Variation of the cubic lattice parameter during the first discharge process.

the surface. Indeed, no incontinuous anomaly can be found in the bulk expansion during the discharge (Figs. 4 and 5).

The large irreversible capacity may also indicate the formation of SEI layer. Fig. 8 shows the repeated charge–discharge curves of nano-sized γ-Fe_2O_3 under the current density of 100 μA cm^{-2}. The reaction is reversible, but huge irreversible capacity of over 140 mAh g^{-1} was observed at the first discharge process, and the subsequent capacity decreases upon repeated cycling is precipitous. Another possible reason of the large irreversible capacity and poor cycle performance may lie in the large difference in particle size between γ-Fe_2O_3 (∼7 nm) and acetylene black (∼35 nm). Efficient formation of the dense nano electron network with intimate contact would be an important future subject.

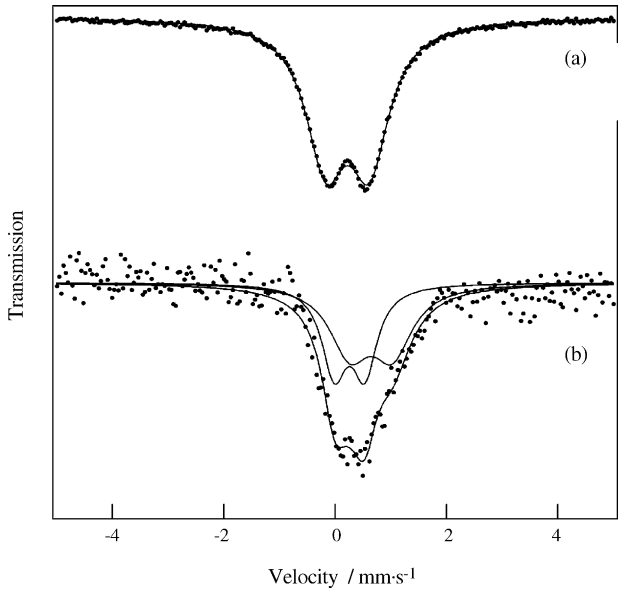

Fig. 7. Mössbauer spectrum for nano-sized γ-Fe_2O_3 (a) before discharge process and (b) after discharge process at 56.5 μA cm^{-2} down to 1.0 V vs. Li/Li^+.

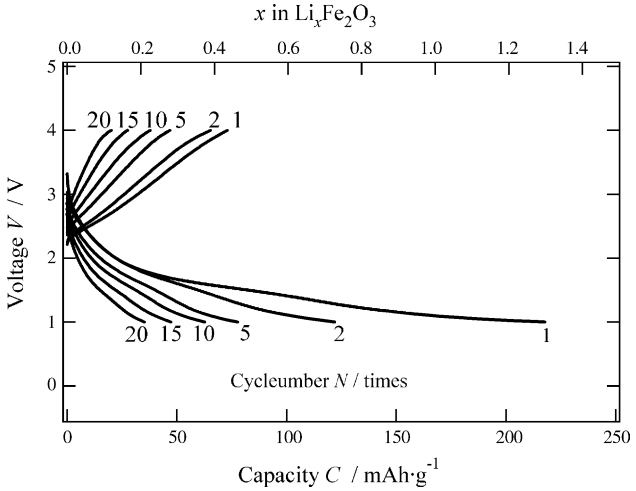

Fig. 8. Repeated charge–discharge curves for nano-sized γ-Fe_2O_3. Current density: 0.1 mA cm^{-2}.

4. Conclusion

Nano-sized γ-Fe_2O_3 with ∼7 nm diameter was successively synthesized using the mild oxidation process of $Fe(CO)_5$. Careful identification of the optimum heat treatment condition was essential to isolate pure γ-Fe_2O_3 phase by the decomposition of the residual organic compounds. Nano-sized morphology led to the large capacity with improved reversibility based on the topochemical lithium intercalation without spinel-rocksalt transformation.

References

[1] M.M. Thackeray, W.I.F. David, J.B. Goodenough, Mater. Res. Bull. 17 (1982) 785.
[2] M. Pernet, J. Rodriguez, M. Gonderand, J. Fontcuberta, P. Strobel, J.C. Joubert, in: Proceedings of ICF-5, 1989, India.
[3] B. Bonnet, P. Strobrl, M. Pernet, M. Gondrand, Y. Gros, C. Mouget, Y. Chaber, Mater. Sci. Forum 91–93 (1992) 345.
[4] D. Larcher, C. Masquelier, D. Bonnin, Y. Chabre, V. Masson, J.-B. Leriche, J.-M. Tarascon, J. Electrochem. Soc. 150 (2003) A133.
[5] D. Larcher, D. Bonnin, R. Cortes, I. Rivals, L. Personnaz, J.-M. Tarascon, J. Electrochem. Soc. 150 (2003) A1643.
[6] T. Matsumura, N. Sonoyama, R. Kanno, M. Takano, Solid State Ionics 158 (2003) 253.
[7] S. Komaba, K. Suzuki, N. Kumagai, Electrochemistry 70 (7) (2002) 506.
[8] S. Ito, K. Ui, N. Koura, K. Akashi, Solid State Ionics 113–115 (1998) 17.
[9] S. Ito, T. Aoyama, K. Akashi, Solid State Ionics 113–115 (1998) 23.
[10] T. Hyeon, S.S. Lee, J. Park, Y. Chung, H.B. Ma, J. Am. Chem. Soc. 123 (2001) 12798.